



HAL
open science

Compact groups from semi-analytical models of galaxy formation - II. Different assembly channels

E. Díaz-Giménez, A. Zandivarez, G. A. Mamon

► **To cite this version:**

E. Díaz-Giménez, A. Zandivarez, G. A. Mamon. Compact groups from semi-analytical models of galaxy formation - II. Different assembly channels. *Monthly Notices of the Royal Astronomical Society*, 2021, 503, pp.394-405. 10.1093/mnras/stab535 . insu-03748209

HAL Id: insu-03748209

<https://insu.hal.science/insu-03748209>

Submitted on 2 May 2023

HAL is a multi-disciplinary open access archive for the deposit and dissemination of scientific research documents, whether they are published or not. The documents may come from teaching and research institutions in France or abroad, or from public or private research centers.

L'archive ouverte pluridisciplinaire **HAL**, est destinée au dépôt et à la diffusion de documents scientifiques de niveau recherche, publiés ou non, émanant des établissements d'enseignement et de recherche français ou étrangers, des laboratoires publics ou privés.

Compact groups from semi-analytical models of galaxy formation – II. Different assembly channels

E. Díaz-Giménez ^{1,2}★, A. Zandivarez ^{1,2} and G. A. Mamon ³

¹Universidad Nacional de Córdoba (UNC). Observatorio Astronómico de Córdoba (OAC), Córdoba, X5000BGR, Argentina

²CONICET. Instituto de Astronomía Teórica y Experimental (IATE), Córdoba, X5000BGR, Argentina

³Institut d'Astrophysique de Paris (UMR 7095: CNRS & Sorbonne Université), Paris, 75014, France

Accepted 2021 February 19. Received 2021 February 4; in original form 2020 November 16

ABSTRACT

We study the formation of over 6000 compact groups (CGs) of galaxies identified in mock redshift-space galaxy catalogues built from semi-analytical models of galaxy formation (SAMs) run on the Millennium Simulations. We select CGs of four members in our mock SDSS galaxy catalogues and, for each CG, we trace back in time the real-space positions of the most massive progenitors of their four galaxies. By analysing the evolution of the distance of the galaxy members to the centre of mass of the group, we identify four channels of CG formation. The classification of these assembly channels is performed with an automatic recipe inferred from a preliminary visual inspection and based on the orbit of the galaxy with the fewest number of orbits. Most CGs show late assembly, with the last galaxy arriving on its first or second passage, while only 10–20 per cent form by the gradual contraction of their orbits by dynamical friction, and only a few per cent forming early with little subsequent contraction. However, a SAM from a higher resolution simulation leads to earlier assembly. Assembly histories of CGs also depend on cosmological parameters. At similar resolution, CGs assemble later in SAMs built on parent cosmological simulations of high density parameter. Several observed properties of mock CGs correlate with their assembly history: early-assembling CGs are smaller, with shorter crossing times, and greater magnitude gaps between their brightest two members, and their brightest galaxies have smaller spatial offsets and are more passive.

Key words: methods: numerical – galaxies: groups: general – galaxies: statistics.

1 INTRODUCTION

Isolated compact groups (CGs) of galaxies constitute an extreme environment, and a unique test-bed for galaxy interactions. Indeed, these high apparent density and low velocity dispersions systems (Hickson et al. 1992) make them ideal laboratories for galaxy interactions and in particular mergers (Mamon 1992). In turn, these interactions induce important transformations that have a strong impact on the history of their galaxy members.

For years, astronomers have been puzzled on how these small systems of galaxies can survive long periods of time and not ending up merging into a single massive galaxy. Numerous N -body simulations have been carried out to answer this question (e.g. Carnevali, Cavaliere & Santangelo 1981; Barnes 1985; Mamon 1987; Navarro, Mosconi & Garcia Lambas 1987; Bode, Cohn & Luggner 1993; Athanassoula, Makino & Bosma 1997), and generally agree that the galaxies rapidly merge over a time-scale of 0.5 to 2 Gyr (see Mamon 1990 for a quantitative comparison of the results of the early simulations). If we observe CGs that do not survive long, a possible explanation for their existence today could be that the group membership is replenished by newly arriving galaxies (Diaferio, Geller & Ramella 1994), as expected from Press–Schechter (Press & Schechter 1974) theory (Mamon 2000). Nevertheless, under proper

conditions, the merging process can be slowed down and therefore the longevity of these systems is not necessarily an issue.

Still, it is not clear how such dense isolated galaxy systems form in the first place. If CGs seen in the local Universe were as dense when they formed as they appear now, they should have formed at early times ($z > 7$ according to Appendix A or $z > 3$ if the groups are double the size in real space as they appear in projection). Alternatively, CGs may be galaxy systems that only very recently have acquired their fourth luminous member (CGs are defined to have at least four galaxies in a range of 3 mag from the brightest group galaxy). In the same spirit, the fourth member may be on its second arrival. Finally, CGs may assemble when galaxies in a group lose their orbital energy and angular momentum by dynamical friction and spiral in to the inner part of virialized groups (e.g. Schneider & Gunn 1982; Ponman et al. 1996).

The assembly history of CGs is best explored with a very comprehensive numerical study. A suitable tool for such a study is the mock galaxy catalogue constructed using semi-analytical models of galaxy formation (SAMs) on top of an N -body cosmological simulation. During the last decade, such mock catalogues built from SAMs have been widely used to understand the frequency, nature, and identification of CGs (McConnachie, Ellison & Patton 2008; Díaz-Giménez & Mamon 2010; Zandivarez et al. 2014b; Díaz-Giménez & Zandivarez 2015; Taverna et al. 2016; Díaz-Giménez, Zandivarez & Taverna 2018), as well as their mass assembly (Farhang et al. 2017) and their frequency versus time (Wiens et al. 2019). The

* E-mail: eugenia.diaz@unc.edu.ar

Table 1. Semi-analytical models analysed in this work.

Authors	Acronym	Cosmology				Simulation		Light-cone		
		Name	Ω_m	h	σ_8	Name	Box size	Galaxies	CGs	CG4s
(1)	(2)	(3)	(4)	(5)	(6)	(7)	(8)	(9)	(10)	(11)
De Lucia & Blaizot (2007)	DLB	WMAP1	0.25	0.73	0.90	MS I	500	3 757 143	3387	1908
Guo et al. (2011)	G11	WMAP1	0.25	0.73	0.90	MS I	500	3 149 024	3175	1570
Guo et al. (2011)	GII	WMAP1	0.25	0.73	0.90	MS II	100	3 214 602	2558	1195
Guo et al. (2013)	G13	WMAP7	0.27	0.70	0.81	MS I	500	2 982 462	1682	1010
Henriques et al. (2015)*	H15	Planck	0.31	0.67	0.83	MS I	480	3 087 401	1291	764

Notes. The columns are: (1): authors; (2): acronym of SAM; (3): cosmology of parent simulation; (4): density parameter of parent simulation; (5): dimensionless $z = 0$ Hubble constant of parent simulation; (6): standard deviation of the (linearly extrapolated to $z = 0$) power spectrum on the scale of $8 h^{-1}$ Mpc; (7): name of parent simulation (MS I = Millennium Simulation I, MS II = Millennium Simulation II); (8): periodic box size of parent simulation [h^{-1} Mpc]; (9): number of galaxies in the mock light-cone; (10): total number of compact groups identified in the mock light-cones ($r \leq 17.77$); (11): the number of compact groups with only four galaxy members.

More accurate values for the simulations can be found at <http://gavo.mpa-garching.mpg.de/Millennium/Help/simulation>.

*H15 is run on a rescaled version of the original Millennium Simulation (hence, the different box size).

nature of CGs has also been analysed from mock CGs extracted from hydrodynamical simulations (Hartuik & Ploekinger 2020).

Tzanavaris et al. (2019) analysed the evolutionary history of a handful of groups identified in 3D as small, dense, and isolated systems inspired in the observational criteria of CGs. Despite their small number of groups (one quintet, one quartet, and eight triplets), they visualized a variety of possible evolutionary paths suggesting that CGs form via different assembly channels, where all galaxies end up lying within 0.5 Mpc from the most massive galaxy within the last 9 to 1 Gyr.

We have recently performed a comprehensive study of the frequency and nature of CGs identified in nine mock light-cones constructed from five different SAMs (Díaz-Giménez et al. 2020, hereafter Paper I). We found that the frequency and nature of CGs depend strongly on the cosmological parameters of the parent dissipationless cosmological simulation on which the SAM had been run. The space density of physically dense CGs increases as a strong power of the amplitude of the power spectrum of primordial density fluctuations on the comoving scale of $8 h$ Mpc, σ_8 . Furthermore, the fraction of CGs that are not physically dense systems of at least four galaxies of comparable luminosity, but instead caused by chance alignments of galaxies along the line of sight, increases with the cosmological density parameter, Ω_m . In currently favoured cosmologies (e.g. WMAP9, Hinshaw et al. 2013 and Planck, Planck Collaboration VI 2020), only roughly 35 per cent of CGs are physically dense (in rough agreement with early estimates by Mamon 1986, 1987). But higher resolution N -body cosmological simulations capture better the formation of physically dense CGs, which now represent roughly half of all CGs. In Paper I, we also found that intrinsic differences in the SAM recipes also lead to differences in the frequency and nature of CGs.

In the present article, we address the following questions. Which is the principal formation channel of CGs: did they assemble early and keep their density, did they gradually increase in density, or did the last galaxy arrive just now on its first or second passage? Is there a mix of CG assembly scenarios? How do cosmological parameters affect CG formation? If CG formation channels are mixed, are there links between specific channels and observational properties of CGs?

To answer these questions, we explore the formation channels of CGs by analysing the mock CG samples we built from the Millennium Simulations (Springel et al. 2005; Boylan-Kolchin et al. 2009) in Paper I. Using the galaxy merger trees from the SAMs, we then follow back in time the most massive progenitors of each of the member galaxies to study the spatial evolution of CGs.

The layout of this work is as follows. In Section 2, we present the SAMs and the light-cone construction from these SAMs. We explain in Section 3 how we built the mock CG sample. Evolutionary tracks are illustrated and classified in Section 4. The statistics of the formation scenarios are presented in Section 5, while their links to observational properties are explored in Section 6. We conclude and discuss our results in Section 7.

2 MOCK GALAXY LIGHT-CONES

We used four SAMs run on the Millennium Simulation (MS I, Springel et al. 2005): those of De Lucia & Blaizot (2007) and Guo et al. (2011) based on cosmological simulations in the WMAP1 cosmology (Spergel et al. 2003); that of Guo et al. (2013) in the WMAP7 cosmology (Komatsu et al. 2011); and the SAM of Henriques et al. (2015) run on the Millennium Simulation rescaled to the Planck cosmology (Planck Collaboration XIII 2016). These SAMs allow us to study the effect of cosmology on CGs formation channels. Moreover, we also used the SAM of Guo et al. (2011) with the WMAP1 cosmology run on the Millennium Simulation II (MS II, Boylan-Kolchin et al. 2009) to understand the effects of space and mass resolution on the CG formation channels. Table 1 lists the different SAMs with their cosmological parameters and parent simulations.

Mock CGs extracted from these SAMs were previously analysed to infer how CG properties depend on the underlying cosmological parameters, spatial and mass resolutions, as well as on the physical properties of the SAM (Paper I). Adopting the procedure of previous works (Guo et al. 2011; Knebe et al. 2015; Irodoutou et al. 2019), we only considered galaxies with stellar masses larger than $\sim 10^9 M_\odot$ ($7 \times 10^8 h^{-1} M_\odot$) for the MS I SAMs, and stellar masses larger than $\sim 10^8 M_\odot$ ($7 \times 10^7 h^{-1} M_\odot$) for the MS II SAM (see queries to retrieve these data in the Appendix of Paper I).

For each SAM listed in Table 1, we constructed all-sky mock galaxy light-cones following a similar procedure as Zandivarez et al. (2014a), using synthetic galaxies extracted from different outputs of the simulations to include the evolution of structures and galaxy properties with time. To compute the observer-frame apparent magnitudes, we applied a k -deconvolution procedure following the recipes described in Díaz-Giménez, Zandivarez & Taverna (2018). Our light-cones are limited to an apparent observer-frame Sloan Digital Sky Survey (SDSS) AB magnitude of $r \leq 17.77$. The total number of galaxies in the light-cone for each SAM is quoted in Table 1. The stellar-mass resolution of each SAM causes the luminosity distributions to be incomplete below a certain value

(see fig. 2 of Paper I). Nevertheless, given the apparent magnitude limit used for building light-cones, the luminosity incompleteness is only present for a very small volume in the nearby universe (~ 0.35 per cent of the light-cone volume for the MS I based SAMs).

3 COMPACT GROUP SAMPLE

We use the samples of mock CGs that we previously identified in these mock galaxy catalogues (Paper I). CGs were identified using the recent CG finding algorithm of Díaz-Giménez et al. (2018). The CG finder looks for groups that simultaneously satisfy constraints of membership, flux limit of the brightest galaxy, compactness, isolation, and velocity concordance. This algorithm is much more efficient, because previous algorithms, based upon selection of CGs projected on the sky (Hickson 1982) followed by the removal of discordant redshifts (Hickson et al. 1992), discard many CGs that appear non-isolated by the presence of neighbouring galaxies that would later turn out to have discordant redshifts. The algorithm also takes into account that the synthetic galaxies are point-sized particles, since galaxies lying very close on the sky in observed CGs may be blended (see Díaz-Giménez & Mamon 2010).

We, hereafter, limit our analyses to CGs of four galaxies (hereafter, CG4s), because assembly histories are simpler when the final number of galaxies is the same. Table 1 indicates that CGs of four galaxies constitute 47 per cent to 60 per cent of the total sample of CGs (decreasing with improved resolution).¹ The relative differences in the number of CG4s in each SAM resembles those of the CGs (including higher richness groups) previously analysed in Paper I.

The Hickson-like automatic search identifies systems that can hardly be considered as dense structures in 3D space (McConnachie, Ellison & Patton 2008; Díaz-Giménez & Mamon 2010). These ‘Fake’ groups have a large maximum 3D separation between their galaxies at $z = 0$ ($> 1 h^{-1}$ Mpc) or they have no close pairs in 3D space (within $200 h^{-1}$ kpc), which makes them unphysical systems. Therefore, Fake CG4s will not be followed back in time to trace their history, and we will consider them as a separate class when needed.

4 CG ASSEMBLY: A TEST SAMPLE

Before analysing all 6447 CG4s, we restricted our analysis to a *test sample* of 342 CG4s, built by selecting ~ 5 per cent of the CG4s of each SAM. In the test sample, we excluded the Fake CGs.

In our analyses, we tracked the evolutionary path of each $z = 0$ galaxy member of the test sample. From the MS data base,² we retrieved the merger history of each of these galaxies using the query example G2 provided in the data base. We then selected only the main progenitor of each $z = 0$ galaxy (main branch of the merger tree) up to the redshift where the galaxy is formed.

At each snapshot, CG4s are characterized by:

- (i) the centre of stellar mass $\mathbf{r}_{\text{cm}} = \frac{\sum_{i=1}^{n=4} \mathcal{M}_i^* \mathbf{r}_i}{\sum_{i=1}^{n=4} \mathcal{M}_i^*}$, where \mathbf{r}_i is the Cartesian vector from the origin of the box to each galaxy member;

¹In our samples of CGs, we deal with two different numbers of member galaxies: the *observed* number and the *real* number. The observed number of members takes into account the blending of galaxies that occurs when two particles in the simulation are too close in projection. For example, a CG with five members may appear as a CG of four observed members if one galaxy is blended with another. In this work, we use the real number of members when defining CG4s.

²<http://gavo.mpa-garching.mpg.de/Millennium/>

- (ii) the module of the comoving 3D distance of each member to the centre of mass. We name this parameter d_i ;

- (iii) the module of the physical 3D distance to the centre of mass computed as $p_i = \frac{d_i}{1 + z_{\text{snapshot}}}$;

4.1 Visual analysis of CG assembly histories

We observed four different types of CG assembly channels:

Late Assembly: the fourth galaxy has just arrived in the CG for the first time (**Late**).

Late Second Pericentre: the fourth galaxy has arrived in the CG on its second passage (**Second**).

Gradual Contraction: the four galaxies might or might not be together since an early epoch, but they have already completed two or more orbits together, becoming gradually closer with each orbit (**Gradual**).

Early Assembly: the four galaxies are together since an early epoch (hereafter **Early**).

Fig. 1 displays examples of these four CG assembly classes extracted from the test sample. The first example, **Late Assembly**, shows that the last galaxy (in black) arrived from a physical distance of roughly $1 h^{-1}$ Mpc. The second example, **Late Second Pericentre**, shows a dense triplet (all galaxies but the black one) forming around 8 Gyr ago ($z = 1.2$) and gradually becoming denser with time, while the last arrival entered the group 3.5 Gyr ago (from a physical distance of $500 h^{-1}$ kpc), bounced out to nearly $200 h^{-1}$ kpc and fell back into the group at $\sim z = 0$, lying $40 h^{-1}$ kpc from the centre. The third example, **Gradual Contraction**, shows a CG that forms between 6 and 5 Gyr ago, and the orbits gradually decay. The fourth example, **Early Assembly**, shows that the CG is already in place 9 Gyr ago, keeping its size ($p_{\text{max}} \simeq 100 h^{-1}$ kpc) since that time.

From the visual classification of the test sample CG4s, we found that 32 per cent are **Late**, 33 per cent are **Second**, 24 per cent **Gradual**, and 11 per cent **Early**.

Fig. 2 shows the frequency of the four CG assembly classes among the test sample of CG4s (blue solid lines), separately for our five considered SAMs. This first attempt of classification shows a tendency to a predominant percentage of recently formed CG4s in those SAMs run on the MS I. In the GII SAM run on the MS II, the fractions of CG4s classified as **Early** and **Gradual** are enhanced by a factor two, and the **Gradual** class is dominant. However, the fractions of assembly classes found with the visually classified test sample should be taken with caution, because of its small number of CGs.

4.2 Automatic classification of CG assembly histories

Our sample of 6000 CG4s was too large to fully classify by visual means. Instead, we performed an automatic classification of CG assembly histories. We first measured the pericentres and apocentres of each galaxy’s orbit relative to the centre of mass of the group. We defined pericentres as those points in the profiles where the steep changes from negative to positive, but also we only considered ‘deep’ pericentres, i.e. there has to be a decay of 20 per cent in the height of the profile when considering the two previous and posterior snapshots. i.e. there is a pericentre in the snapshot j if

$$\frac{p_i(t_{j-2}) - p_i(t_j)}{p_i(t_j)} > 0.2 \text{ AND } \frac{p_i(t_{j+2}) - p_i(t_j)}{p_i(t_j)} > 0.2. \quad (1)$$

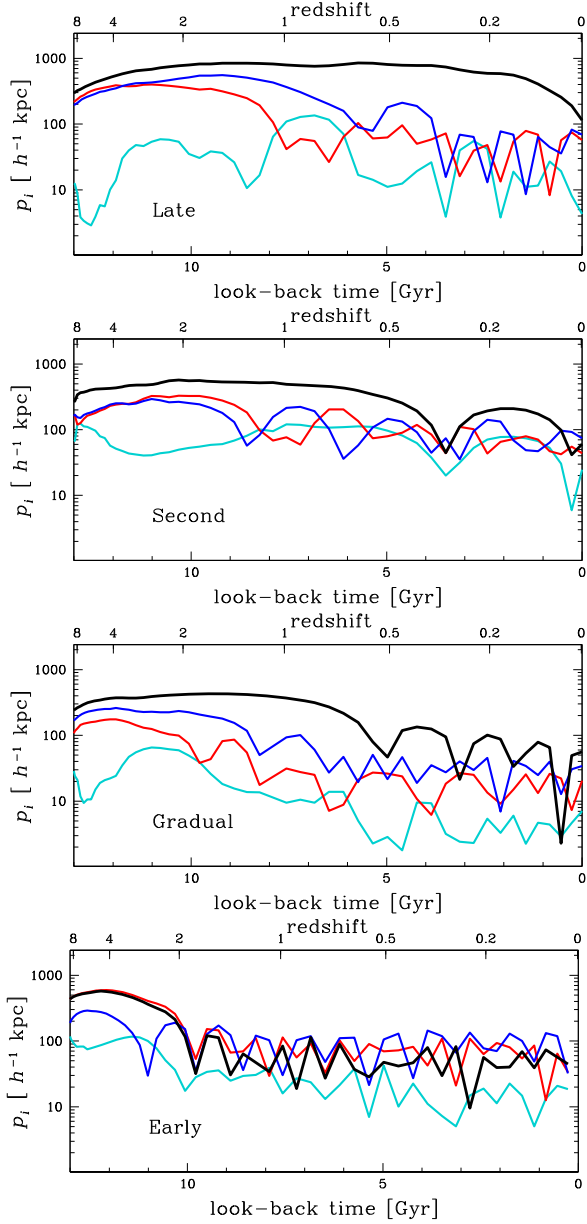


Figure 1. Assembly histories of four CG4s, defined by the main progenitors of their $z = 0$ galaxies, traced by the evolution of the 3D physical distance of each galaxy member to the CG centre of mass. Time (age of the Universe) increases towards the right. The four rows highlight examples of the Late, Second, Gradual, and Early CG assembly classes, from top to bottom. The black lines display the key galaxies indicating the formation channel. The physical separation between two galaxies at a given look-back time is at most the sum of their p_i values (since they may lie on opposite sides of the CG centre of mass).

The apocentres are the highest values of $p_i(t)$ in the profiles between two consecutive pericentres.

The profiles of each galaxy member are characterized by the following ten parameters:

- (i) t_{1p} : time of the first (earliest) pericentre;
- (ii) h_{1p} : p_i at the time of the first pericentre;
- (iii) t_{lp} : time of the last pericentre;
- (iv) h_{lp} : p_i at the time of the last pericentre;
- (v) t_{1a} : time of the first apocentre;

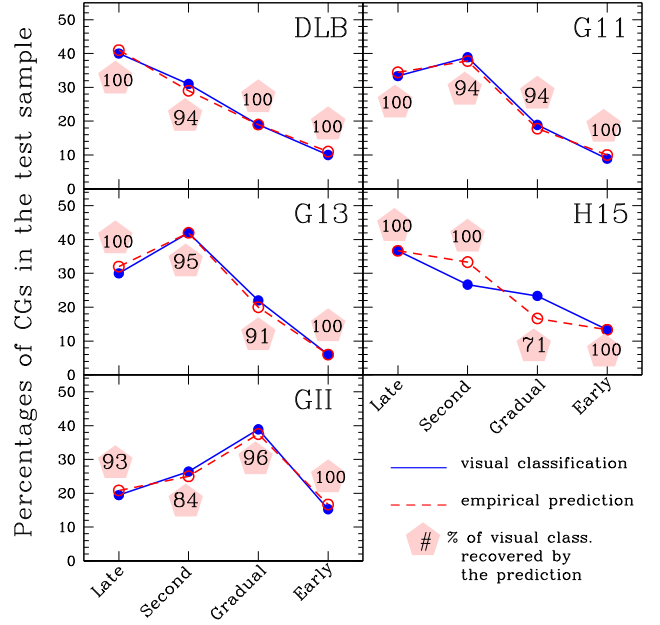


Figure 2. Distributions of assembly classes for the test sample of $z = 0$ 4-galaxy CGs, for the five different semi-analytical models. The results of the visual and empirical classifications are shown as blue filled circles and solid lines and red open circles and dashed lines, respectively. Inset numbers show the percentages of the visual classification recovered by the automatic prediction in each class.

- (vi) h_{1a} : p_i at the time of the first apocentre;
- (vii) t_{1a} : time of the last apocentre;
- (viii) h_{la} : p_i at the time of the last apocentre;
- (ix) n_p : total number of deep pericentres (defined in equation 1);
- (x) $p(t_0)/p(t_1)$: ratio between the p_i in the two latest snapshots.

Following the insights from the observations of the individual galaxy profiles, we characterize the assembly history of a CG4 by selecting the *key galaxy* as the member with the fewest number of orbits, i.e. the lowest value of n_p (black lines in Fig. 1). In those cases where two or more galaxies present the same number of pericentres, we defined the key galaxy as the galaxy with the most recent t_{1p} provided that those times differ in more than 1 Gyr. When the latest requirement was not fulfilled, we defined the key galaxy as that with the highest h_{1p} .

Analysing different combinations of features in the profile of the key galaxy, we realize that our visual classification relies mainly on a few parameters of the profiles. In Fig. 3, we show the scatter plots (as heat diagrams) of the number of pericentres in the key galaxy profile versus the look-back time of its first pericentre (top row), and versus the ratio $p(t_0)/p(t_1)$, for groups split according to their visual classification (columns). Based on these correlations, we propound the following automatic classification:

$$\begin{aligned}
 &\text{Late: } t_{1p} < 7.5 \text{ Gyr AND} \\
 &\{n_p = 0 \text{ OR } [n_p = 1 \text{ AND } p(t_0) > p(t_1)]\} \\
 &\text{Second: } t_{1p} < 7.5 \text{ Gyr AND} \\
 &\{[n_p = 1 \text{ AND } p(t_0) \leq p(t_1)] \text{ OR } [n_p = 2 \text{ AND } p(t_0) > p(t_1)]\} \\
 &\text{Gradual: } t_{1p} < 7.5 \text{ Gyr AND} \\
 &\{[n_p = 2 \text{ AND } p(t_0) \leq p(t_1)] \text{ OR } n_p > 2\} \\
 &\text{Early: } t_{1p} \geq 7.5 \text{ Gyr}
 \end{aligned}$$

Note that this classification does not involve any physical size.

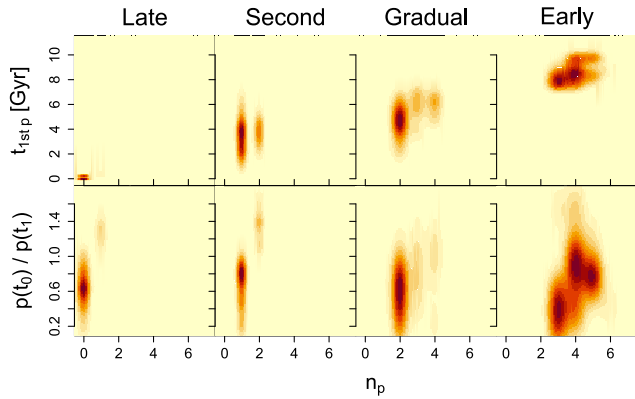


Figure 3. Heat diagrams for the scatter plots of look-back time of the first pericentre (*top row*) and ratio of the sizes of the profile at the latest times (*bottom row*) both versus the number of pericentres, for the key galaxies of the test sample split into different assembly channels according to the visual classification.

The application of this automatic classification to our test sample led to 96 per cent success at recovering the visual classification (the success rates within each SAM are 98, 97, 96, 93, and 93 for DLB, G11, G13, H15, and GII, respectively). The success rates as a function of visual class are 99, 93, 94, and 100 per cent for Late, Second, Gradual, and Early, respectively.

Fig. 2 shows that the automatic classification applied to the test sample (red dashed lines) follows very well the visual classification (blue solid lines). In Fig. 2, we also display the percentage of visually classified test CG4s that match the predictions from the automatic classification for each class of formation channels. These percentages of agreement are above 90 per cent and often 100 per cent, except for two among 20 cases: the Gradual class with the H15 SAM (71 per cent) and the Second class with the GII SAM (84 per cent). We, therefore, conclude that the predictions obtained from the automatic recipe reproduce the visual classifications of test CG4s with excellent fidelity.

5 RESULTS ON COMPACT GROUP FORMATION CHANNELS

Given the high success rate achieved by the automatic classification, we applied it to the entire sample of CG4s. Fig. 4 shows the percentage of CG4s within each formation channel. Roughly 20 per cent of the CG4s are classified as Fake. This figure shows some differences with those from the smaller test sample (dashed lines in Fig. 2), which suffers from worse statistics. However, regardless of the SAMs, the tendency of the predominant recent formation of CG4s is confirmed and the percentage of CGs diminishes towards the earlier assembly channels. Between one-third and one-half of the CG4s are Late, while less than a tenth are Early systems.

5.1 Physically dense and chance alignments CGs

We split the samples of CG4s into *physically dense* (Reals) and *chance alignments* (CAs) following the classification of Díaz-Giménez & Mamon (2010). Real CGs are those whose maximum comoving 3D separation between the four closest galaxies is less than $100 h^{-1}$ kpc, or less than $200 h^{-1}$ kpc if the ratio of line of sight to transverse sizes in real space is less than 2. The remaining

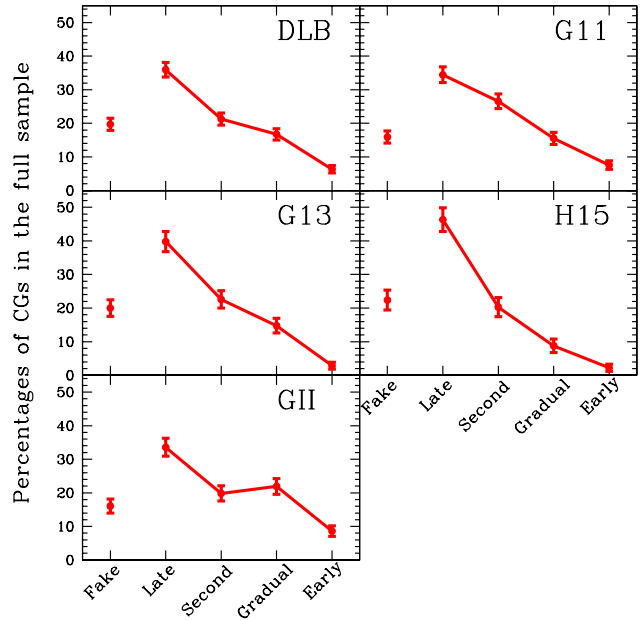


Figure 4. Percentages of $z = 0$ 4-galaxy CG assembly channels in the full sample, for the five different semi-analytical models, using the automatic classification. The percentages of CGs that are Fake are also shown. Error bars are the 95 per cent binomial confidence intervals.

Table 2. Number of $z = 0$ CGs with only four members for each class.

SAM	CG4 Total	Reals		CAs	
		Total	%	Total	Fake
All	6447	2024	31	4423	1191
DLB	1908	588	31	1320	376
G11	1570	530	34	1040	250
G13	1010	300	30	710	202
H15	764	185	24	579	171
GII	1195	421	35	774	192

CGs are classified as CAs. In this scenario, the Fake CGs defined in Section 3 belong to the CA subsample.

The numbers of different classes of CG4s identified in each light-cone are listed in Table 2. One first notices that the fraction of Reals among CG4s is typically 30 per cent lower than the corresponding fraction among all CGs given in the top panel of fig. 8 of Paper I. In particular, among CG4s, the fraction of Reals never exceeds 35 per cent (reached for GII).

In addition, in Fig. 5, we show the percentage of Reals and CAs within each formation channel. Regardless of the SAM, over three-quarters of the Late forming CGs are CAs; CAs are also the dominant population within the Second channel, while the Reals dominate the Early assembly CGs. In Appendix B1, we focused on the CA CG4s by analysing their internal substructures. Among the few CAs that formed earlier, the CAs formed by a triplet plus a somewhat distant galaxy are the main contributors to the long-lived classes (Fig. B1).

Fig. 6 displays the percentages of different CG assembly channels among Reals and CAs. The assembly histories of Real CGs depend somewhat on the SAM. Real CGs in the DLB and GII SAMs are mainly assembled gradually, while in G11 and G13, Real CGs present a homogeneous mixture of Late, Second, and Gradual

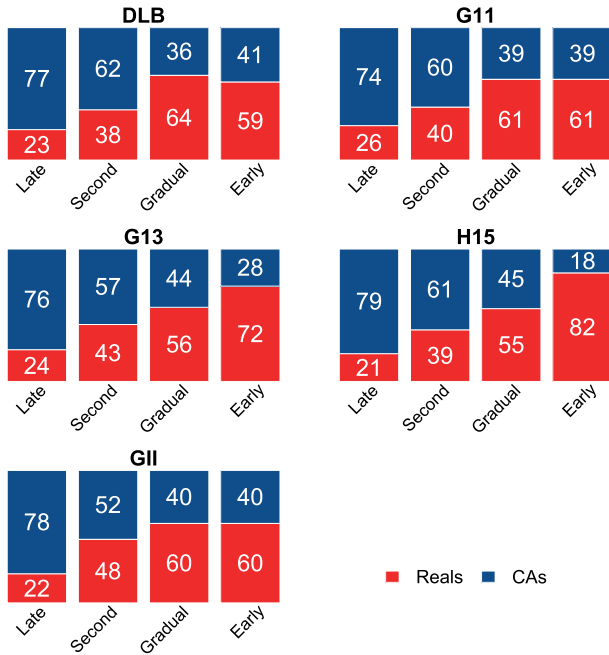


Figure 5. Percentage of Reals and CAs (including Fakes) within each formation channel.

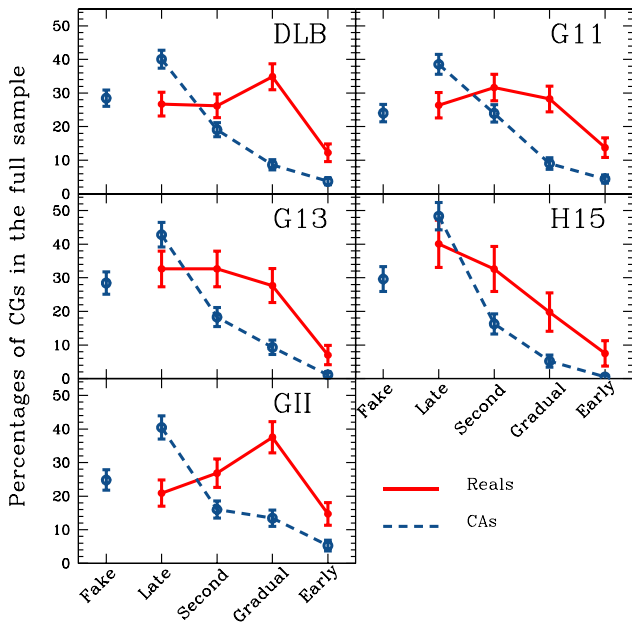


Figure 6. Percentages of $z = 0$ 4-galaxy CG assembly channels for Real and chance-alignment CGs (including Fakes) in the full sample (red and blue, respectively), for the five different semi-analytical models, using the automatic classification. The percentages of CAs that are Fake are also shown. Error bars are the 95 per cent binomial confidence intervals.

classes. Finally, Real CGs in the H15 SAM are dominated by recently assembled CGs.

Fig. 6 indicates that, regardless of the SAM, CAs assemble significantly more recently than Real CG4s. Indeed, the Late class of assembly history accounts for a significantly higher fraction of CAs (typically over 40 per cent) than of Reals (typically under 30 per cent).

5.2 Dependence on cosmology and SAM recipes

Following Paper I, we explore the dependence of our results with the underlying cosmological parameters of the SAMs and with their physical recipes. Fig. 7 shows the fraction of a composite assembly class named *Earlies*, which combines Gradual and Early classes, as a function of cosmological parameters and the fraction of orphan galaxies in each SAM. We estimate the power-law relations for the fraction of *Earlies*: Ω_m^α , σ_8^β , and f_{orph}^γ . The fits were obtained using all the SAMs with the same resolution (MS I). The best-fitting values of the exponents are quoted in the figure.

We first noted some trends of CG assembly classes with cosmological parameters. SAMs built in denser universes (G13 and especially H15) have lower fractions of *Earlies*. On the other hand, there is only a weak positive trend of the assembly history as a function of the amplitude of mass fluctuations (σ_8). We discuss these trends in Section 7 below.

Contreras et al. (2013) and Pujol et al. (2017) observed that differences in the treatment of orphan galaxies in the SAMs impact on the small-scale clustering of galaxies, which are the relevant scales for CGs. Orphan galaxies are those whose subhaloes became no longer sufficiently massive to be realistic or no longer visible at all. The SAMs can no longer use the subhaloes to follow their positions and rely instead on crude recipes for their orbital evolution. Hence, the treatment of orphans implemented in each SAM affects the abundance of this particular population of satellite galaxies.

In Paper I, we noticed that orphan galaxies are frequent in CGs, especially Real ones. We also found that the fraction of CGs that are physically dense (i.e. Reals) decreases with the fraction of orphans in the SAMs for given cosmological parameters, but increases with orphan fraction for given resolution. We therefore analysed the fraction of *Earlies* as a function of the fraction of orphan galaxies in the light-cones built from each SAM (right-hand panels of Fig. 7).

Considering SAMs obtained from the MS I simulation (i.e. all with the similar mass resolution), Fig. 7 shows that the fraction of *Earlies* increases with the fraction of orphan galaxies. This trend appears to be statistically significant in Reals and even more pronounced in CAs. As noted in Paper I, lower fractions of orphan galaxies are found in mocks from SAMs run on the higher resolution MS II simulation. Indeed, such simulations allow following the orbits of low-mass galaxies, which tend to live in lower subhalo masses, instead of having to predict them with uncertain dynamical recipes. From this figure, it can be seen that despite the lower fraction of orphans, a higher fraction of *Earlies* is found in the MS II, similar to the fraction of *Earlies* in the comparable G11 SAM. This suggests that orphans play a minor role in comparison with Ω_m in setting the fraction of CG4s assembling early.

Our classification is based on the orbits of key galaxies, some of which require analytical recipes when the subhalo has too few particles or disappears entirely, i.e. for orphan galaxies. We therefore examined the impact of orphan key galaxies within each formation channel, and we show the main results in Fig. 8.

First, we found that, summing over all assembly channels, roughly one-third (or less depending on the SAM) of the key galaxies become orphans at some time in their evolutionary history (top labels). Furthermore, the occurrence of orphan key galaxies increases from the Late to the Early channel. For the MS I based SAMs, the percentage of key galaxies that are orphans rises from ~ 13 per cent in the Late CGs to ~ 85 per cent in the Early CGs. For the better resolved GII SAM, this increase is considerably lower.

From the merger trees of the orphan key galaxies, it is possible to determine the look-back time and the physical distance to the

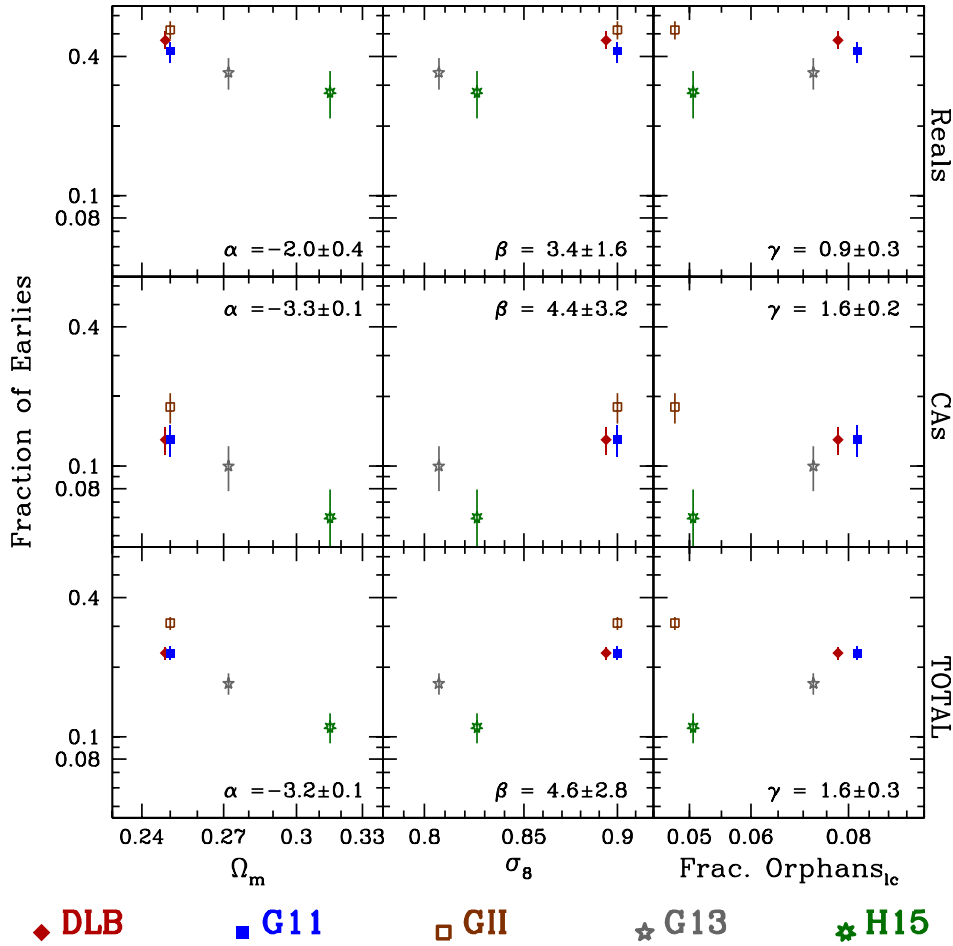


Figure 7. Fraction of $z = 0$ 4-galaxy CGs whose assembly histories are Earlies (Gradual+Early) as a function of the cosmological matter density parameter (Ω_m) (left-hand panels), the amplitude of the mass fluctuations in a sphere of $8 h^{-1}$ Mpc (σ_8) (middle panels), and the fraction of orphan galaxies in the light-cones (right-hand panels). The trends are shown for the subsamples of Real and CA CGs (upper and middle panels) as well as for the total sample (lower panels). The normalizations of CA and total samples include the Fake CGs. In each panel, the values of the slopes of the fits using all MS I are quoted.

mass centre when they became orphans. The median values of these two features are shown in Fig. 8. Typically, the key galaxies in the Second and Gradual channels become orphans during the last 5 Gyr, when they are less than $100 h^{-1}$ kpc from the CG centre (typically less than $50 h^{-1}$ kpc for the better resolved GII SAM). The key galaxies in the Early channel have also become orphans when they are close to the centre, but this occurs earlier. In these three assembly classes, galaxies become orphans at distances to the CG centre of mass of order the half-maximum size of the system ($200 h^{-1}$ kpc) or less (in particular for the better resolved GII SAM, but also for some other cases). Therefore, the assembly into the small CG size typically occurs when the galaxies are not yet orphans, i.e. before the time when the SAMs use analytical recipes to predict galaxy orbits.

On the other hand, the key galaxies in the Late channel became orphans only recently, but at larger distances to the centre. However, the percentage of Late CGs that are classified using an orphan galaxy is very low in all the SAMs.

We conclude that the presence of orphan galaxies as key galaxies does not modify the results found in this work. We also checked whether the visual classification was influenced with the key galaxy being an orphan, but found no clear such influence.

6 ARE OBSERVED CG PROPERTIES LINKED TO THEIR ASSEMBLY HISTORY?

One may wonder whether observational properties of CG4s may retain signatures of their particular assembly history.

Fig. 9 shows the distribution of different properties of CG4s in the GII SAM in form of boxplot diagrams (similar plots for CG4s in the other four SAMs are shown in Fig. B2). The dimensionless group crossing time and group virial theorem mass-to-light ratio are measured as Díaz-Giménez et al. (2012): $H_0 t_{\text{cr}} = 50 (\pi/\sqrt{3}) (h d_{ij}/\sigma_v)$ and $M_{\text{VT}}/L = 3\pi (d_{ij}^{-1})^{-1} \sigma_v^2/(G L)$, where d_{ij} is the median intergalaxy separation projected on the sky.

Analysing the median values obtained from this figure,³ some dependence of these properties on the assembly class is observed. CG4s in the Early class show the largest magnitude gaps, as well as the lowest projected sizes, crossing times, and brightest galaxy relative projected offsets. Those attributes are actually a good reflection of their early formation times. On the other hand, CG4s

³If the notches in two boxplots do not overlap, one can conclude with 95 per cent confidence that the corresponding medians are different (McGill, Tukey & Larsen 1978; Krzywinski & Altman 2014).

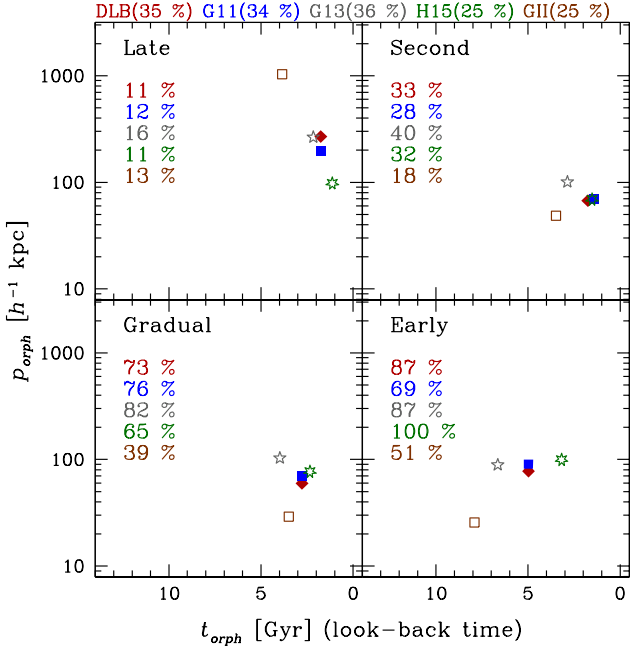


Figure 8. Median (over CGs) positions and times when key galaxies become orphan (they lose their subhaloes and the SAMs treat their orbits within analytical recipes). *Top labels* quote the percentages of CG4s (excluding Fake CGs) in each SAM whose key galaxies became orphans. Each panel corresponds to the different assembly channels. Different *symbols* display the different SAMs, as in Fig. 7. *Inset legends* quote the percentage of CG4s within each assembly channel whose key galaxy became an orphan at some time (from top to bottom: DLB, G11, G13, H15, and GII).

recently formed show the opposite behaviour, with the Late class showing the smallest magnitude gaps, as well as the largest projected sizes, crossing times, and brightest galaxy relative projected offsets.

In general, there seems to be a progression in the median properties between the four group assembly channels, following the trend: Early Assembly, Gradual Contraction, Late Second Pericentre, Late Assembly.

We have also included in this figure the properties of those CG4s classified as Fake to have the complete picture of all CG4s in the main sample. In most of the properties, Fake CG4s behave similarly to the recently formed CG4s, except for the crossing times where Fake CG4s have lower values.

While Fig. 9 shows this analysis only for the GII SAM, roughly the same trends are observed for all the remaining SAMs (see Fig. B2). Moreover, Figs 9 and B2 show that all SAMs display weaker but apparently significant trends for Early assembly histories for CGs of higher group velocity dispersion and higher brightest galaxy stellar mass-to-luminosity ratio. In contrast, contradictory trends among the CG4s built from the different SAMs are found for group luminosity and virial-theorem-mass-to-luminosity ratio.

7 SUMMARY AND DISCUSSION

In this work, we studied the different assembly channels that give rise to the CGs of galaxies identified at present using an automatic algorithm that follows Hickson’s well-known recipes (Hickson 1982; Hickson et al. 1992). Following our previous work (Paper I), we identified CGs in several mock light-cones constructed from the Millennium Simulations using different SAMs. Since our study involves following each member of a CG back in time, we simplified

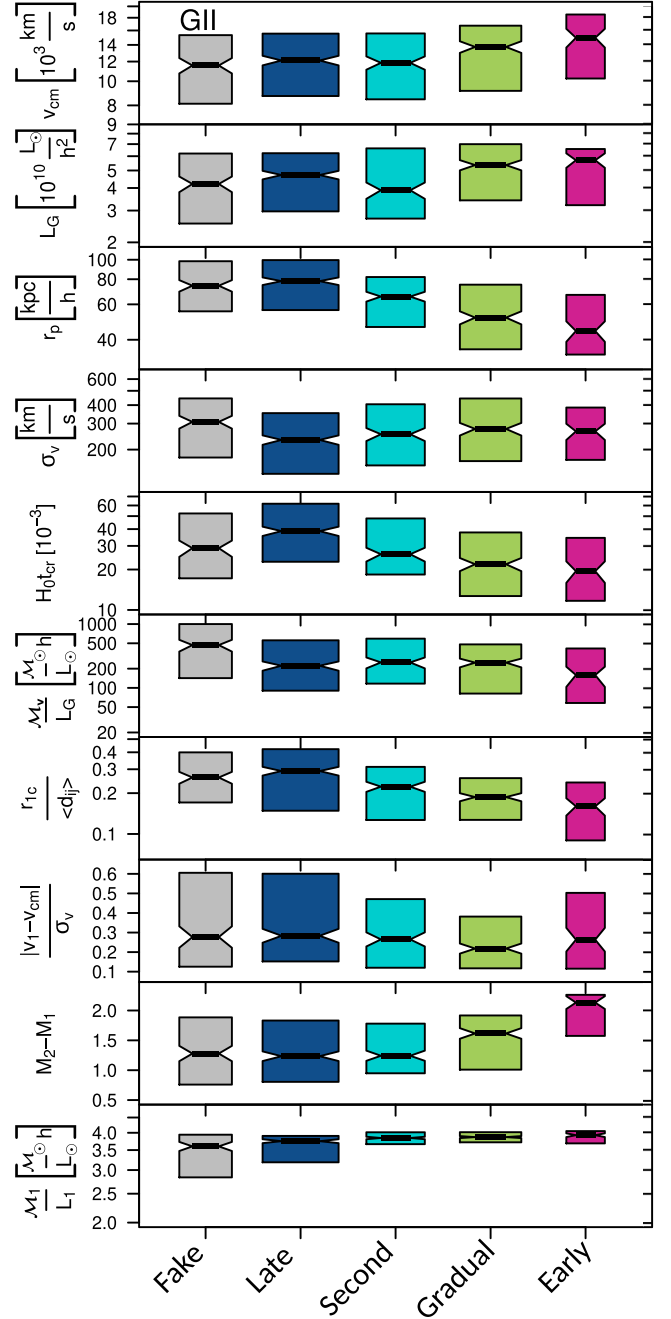


Figure 9. Distribution of the observable properties of $z = 0$ mock 4-galaxy CGs (with no splitting between Real and CAs) as a function of the assembly class for the GII SAM (*second to last columns*). We also include the properties for the sample of CGs previously classified as Fake CAs (*first column*). The properties, from *top to bottom*, are distance (median line-of-sight velocity), group luminosity, projected radius of the minimum enclosing circle, group line-of-sight velocity dispersion, dimensionless group crossing time, group virial theorem mass-to-light ratio, dimensionless brightest galaxy projected group-centric distance, dimensionless brightest galaxy line-of-sight velocity offset, r -band magnitude gap between the two most luminous galaxies, and brightest galaxy stellar mass-to-light ratio. The *waists*, *tops*, and *bottoms* of the *coloured boxes* indicate the median values, and the 75th and 25th percentiles, respectively; the *widths* of the boxes are proportional to the numbers of CGs, while *notches* around the waists show the 95 per cent confidence interval on the medians.

our analysis by only selecting CGs with four members (CG4s), and by only following their most massive progenitors. We thus analysed the assembly histories of over 6000 CG4s in the outputs of five SAMs.

To start with, we performed a preliminary analysis, where we visually inspected a small subset (~ 350 CG4s) of CG assembly histories, using the evolution of the 3D physical distances of galaxy members to the group centre of mass. This allowed us to differentiate four different basic assembly channels that we named *Early Assembly*, *Gradual Contraction*, *Late Assembly*, and *Late Second Pericentre* (Fig. 1). The first two channels encompass relatively old systems, while the last two are characterized by rather late assembly. We notice that there is a wide spectrum of possible variations for the evolution of CG4s, and some of them evolve in ways that are at the boundaries between channels. Therefore, our classification is most probably a simplification. From the analysis of the test sample, we observed a tendency of CG4s to be predominantly recently formed (Fig. 2).

We then extended this analysis to the full sample of CG4s, by defining an automatic classification using some of the features measured on the evolution of the physical 3D distance to the group centre of mass of the galaxy with the fewest significant pericentres (see Fig. 3). This automatic classification achieved a 96 per cent average success rate in recovering the visual classification.

Applying our automatic classification on the full sample of 6000 CGs, we found that recently formed CGs are the dominant assembly class, regardless of the SAMs. When analysing CGs classified as *Reals* according to the classification scheme of Díaz-Giménez & Mamon (2010), we observed that they have, on average, an important component of older systems, whereas CGs that are *Chance Alignments* according to the Díaz-Giménez & Mamon classification are preferentially dominated by recently assembled systems (Fig. 6).

One may wonder what is the meaning of assembly classes of CGs that are chance alignments. There is no bimodality in the 3D properties of CGs: as seen in fig. 6 of Díaz-Giménez & Mamon (2010), our distinction between *Reals* and *CAs* is based on a somewhat arbitrary cut in the smooth distribution of mock CGs in the alignment versus size plane. Many *CAs* barely missed being classified as *Reals*. Therefore, there is no strong reason to exclude *CAs* from the analysis.

Among CGs, *Reals* have greater number density and presumably greater mass density than the *CAs*. The shorter assembly time for the *Reals* relative to the *CAs* is thus related to the shorter assembly times in systems that are denser at $z = 0$.

Cosmological parameters play a strong role on CGs. In Paper I, we had found that the space density of CGs decreases strongly when increasing the density of the Universe. We interpreted this result as the greater contamination of the CG isolation criterion in high-density universes. We had also noted that the fraction of CGs that are *CAs* increases with Ω_m , especially for the *CAs* that extend in real space beyond the parent group of the CG, which indeed should occur more frequently in high-density universes. In this work, we find that the density of the Universe plays a major role on CG4 assembly. Denser flat universes lead to later CG assembly (left-hand panels of Fig. 7). This is the consequence of greater late infall in denser flat universes (van den Bosch 2002).

We also find a marginally strong trend of increasing fraction of *Earlies* in *Real* CGs extracted from SAMs built from high σ_8 cosmologies (middle column of panels of Fig. 7). Increasing the normalization of the power spectrum leads to more structures at all scales. In Paper I, we found that increasing σ_8 leads to a higher fraction of CGs that are *Real*. Fig. 6 indicates that *Real* CG4s assemble earlier than *CAs*. Thus, the weak positive correlation

between fraction of early assembly with σ_8 may be the consequence of the higher fraction of *Reals* and their earlier assembly.

The fraction of early-assembling CGs may depend on the SAM considered. In comparison with DLB, the G11 SAM based on the same cosmological parameters leads to a similar fraction of *Earlies* (Fig. 7). In comparison with G13, H15 has fewer *Earlies*, but it is not clear whether this difference is caused by the SAM physics or by the different cosmological parameters. In fact, G11 and G13 have mostly the same SAM but different cosmological parameters and they show indeed differences in the fraction of *Earlies*. This suggests that SAM physics only plays a minor role in the CG assembly, for given cosmological parameters.

The resolution of the simulation appears to play a role. We compare the fractions of *Earlies* between the high-resolution GII SAM and the comparable lower resolution G11 SAM (same study and cosmological parameters). We find that the fraction of *Earlies* among all CGs is one-third (and significantly) higher for the high-resolution GII. This is expected, because in higher resolution simulations small or low-mass structures form earlier (as do galaxies, see e.g. fig. 11 of Tweed et al. 2018).

Another relevant issue in the SAMs is the way they deal with the orphan galaxies, whose positions are extrapolated with analytical recipes. Thus, if a key galaxy is an orphan, then the assembly channel for its group could be based on such an imprecise extrapolation. Fig. 8 indicates that ~ 30 per cent of the CG4 assembly channel classifications were based on orphan key galaxies. In such cases, galaxies in *Second*, *Gradual*, and *Early* CGs became orphans once the systems were already small. Key galaxies in *Late* CGs were located farther from the group centre when they became orphans, but the percentage of *Late* CGs with orphan key galaxies is rather low. Therefore, we find that having an orphan galaxy as key galaxy to classify the assembly of CGs does not introduce biases in our results.

Finally, we also investigated if the formation channel of CGs has an effect on their observational properties. From the analysis of several observational properties, there seems to be a progression in the median properties: earlier formed CGs tend to be the smallest, densest (shortest crossing times), with the largest magnitude gap between the two brightest members, while more recently formed CGs show the opposite behaviour (Figs 9 and B2).

There are similarities between the correlation of assembly times and observational properties for CG4s and for groups in general. Since the pioneering work of Jones et al. (2003), old galaxy groups have been directly associated with systems showing a large magnitude gap between the two brightest galaxies. This association has been confirmed using galaxies in mock catalogues built from SAMs, not only using the gap between the two brightest galaxies (e.g. Dariush et al. 2007; Díaz-Giménez, Muriel & Mendes de Oliveira 2008), but also using the gap between the first and fourth brightest galaxies (e.g. Dariush et al. 2010; Kanagusuku, Díaz-Giménez & Zandivarez 2016). Other physical quantities have been found to correlate with the epoch of group assembly. Khosroshahi, Ponman & Jones (2007) found that older galaxy systems (with large magnitude gap) have a more concentrated halo compared with those recently formed. In the same vein, Ragono-Figueroa et al. (2010) found that more concentrated groups form earlier in cosmological hydrodynamical simulations. In our work, we found that the four galaxy members in early formed CGs are clearly confined to a smaller region of space than those in recently formed CGs.

Raouf et al. (2014) argued that group assembly history is best measured with a combination of observational parameters: they considered the group and brightest group galaxy (BGG) luminosities and the physical offset of the BGG from the luminosity centroid.

Farhang et al. (2017) found that CGs acquire half their mass earlier than normal groups, but later than Fossil groups. Our results have shown that the findings valid for early-forming galaxy groups also hold for early-assembly CGs (at least for median values), which are denser (shorter crossing times) and whose BGGs have greater magnitude gaps, and lie closer to the luminosity centroid, than later-assembly CGs.

However, our analysis is different from all these studies, because we do not measure the epoch when half of the CG mass is assembled. Instead, we measure the spatial assembly history, which we split into four formation channels. We found that these channels represent themselves an evolutionary sequence that are correlated with observational properties in accordance to what was found for the mass assembly history by the studies mentioned above.

Unfortunately, the median observational properties of CGs split into each of the four formation channels are not sufficiently different to reliably infer the formation channel of individual CGs.

Some issues remain to be clarified. What prevents Early Assembly CGs to gradually shrink in size by dynamical friction and inelastic galaxy–galaxy encounters? Will our results differ when we analyse mock catalogues built from cosmological hydrodynamical simulations (as rapidly done by Hartsuiker & Ploekinger 2020), which now have sufficient spatial resolution to achieve better small-scale physics compared to SAMs? Do the formation channels of four-member CGs differ from those of other (less dense) groups of four members?

ACKNOWLEDGEMENTS

We thank the anonymous referee for useful comments, as well as Matthieu Tricottet. We also thank the authors of the SAMs for making their models publicly available. The Millennium Simulation data bases used in this paper and the web application providing online access to them were constructed as part of the activities of the German Astrophysical Virtual Observatory (GAVO). This work has been partially supported by Consejo Nacional de Investigaciones Científicas y Técnicas de la República Argentina (CONICET) and the Secretaría de Ciencia y Tecnología de la Universidad de Córdoba (SeCyT).

DATA AVAILABILITY

The data underlying this article were accessed from <http://gavo.mpa-garching.mpg.de/Millennium/>. Galaxy light-cones built in Paper I and used in this work are accessed from <https://doi.org/10.7910/DVN/WGOPCO> (Díaz-Giménez et al. 2021). The derived data generated in this research will be shared on reasonable request to the corresponding authors.

REFERENCES

Athanassoula E., Makino J., Bosma A., 1997, *MNRAS*, 286, 825
 Barnes J., 1985, *MNRAS*, 215, 517
 Bode P. W., Cohn H. N., Lugger P. M., 1993, *ApJ*, 416, 17
 Boylan-Kolchin M., Springel V., White S. D. M., Jenkins A., Lemson G., 2009, *MNRAS*, 398, 1150
 Carnevali P., Cavaliere A., Santangelo P., 1981, *ApJ*, 249, 449
 Contreras S., Baugh C. M., Norberg P., Padilla N., 2013, *MNRAS*, 432, 2717
 Dariush A., Khosroshahi H. G., Ponman T. J., Pearce F., Raychaudhury S., Hartley W., 2007, *MNRAS*, 382, 433
 Dariush A. A., Raychaudhury S., Ponman T. J., Khosroshahi H. G., Benson A. J., Bower R. G., Pearce F., 2010, *MNRAS*, 405, 1873
 De Lucia G., Blaizot J., 2007, *MNRAS*, 375, 2
 Diaferio A., Geller M. J., Ramella M., 1994, *AJ*, 107, 868
 Díaz-Giménez E., Mamon G. A., 2010, *MNRAS*, 409, 1227

Díaz-Giménez E., Zandivarez A., 2015, *A&A*, 578, A61
 Díaz-Giménez E., Muriel H., Mendes de Oliveira C., 2008, *A&A*, 490, 965
 Díaz-Giménez E., Mamon G. A., Pacheco M., Mendes de Oliveira C., Alonso M. V., 2012, *MNRAS*, 426, 296
 Díaz-Giménez E., Zandivarez A., Taverna A., 2018, *A&A*, 618, A157
 Díaz-Giménez E., Taverna A., Zandivarez A., Mamon G. A., 2020, *MNRAS*, 492, 2588
 Diaz-Gimenez E., Taverna A., Zandivarez A., Mamon G., 2021, *Galaxy Lightcones*
 Farhang A., Khosroshahi H. G., Mamon G. A., Dariush A. A., Raouf M., 2017, *ApJ*, 840, 58
 Guo Q. et al., 2011, *MNRAS*, 413, 101
 Guo Q., White S., Angulo R. E., Henriques B., Lemson G., Boylan-Kolchin M., Thomas P., Short C., 2013, *MNRAS*, 428, 1351
 Hartsuiker L., Ploekinger S., 2020, *MNRAS*, 491, L66
 Henriques B. M. B., White S. D. M., Thomas P. A., Angulo R., Guo Q., Lemson G., Springel V., Overzier R., 2015, *MNRAS*, 451, 2663
 Hickson P., 1982, *ApJ*, 255, 382
 Hickson P., Mendes de Oliveira C., Huchra J. P., Palumbo G. G., 1992, *ApJ*, 399, 353
 Hinshaw G. et al., 2013, *ApJS*, 208, 19
 Irodou D., Thomas P. A., Henriques B. M., Sargent M. T., Hislop J. M., 2019, *MNRAS*, 489, 3609
 Jones L. R., Ponman T. J., Horton A., Babul A., Ebeling H., Burke D. J., 2003, *MNRAS*, 343, 627
 Kanagusuku M. J., Díaz-Giménez E., Zandivarez A., 2016, *A&A*, 586, A40
 Khosroshahi H. G., Ponman T. J., Jones L. R., 2007, *MNRAS*, 377, 595
 Knebe A. et al., 2015, *MNRAS*, 451, 4029
 Komatsu E. et al., 2011, *ApJS*, 192, 18
 Krzywinski M., Altman N., 2014, *Nat. Methods*, 11, 119
 Mamon G. A., 1986, *ApJ*, 307, 426
 Mamon G. A., 1987, *ApJ*, 321, 622
 Mamon G. A., 1990, in Sulentic J. W., Keel W. C., Telesco C. M., eds, *NASA Conference Publication*, Vol. 3098. NASA Conference Publication, p. 609
 Mamon G. A., 1992, *ApJ*, 401, L3
 Mamon G. A., 2000, in Valtonen M. J., Flynn C., eds, *ASP Conf. Ser. Vol. 209*, IAU Colloq. 174: Small Galaxy Groups. Astron. Soc. Pac., San Francisco, p. 217
 McConnachie A. W., Ellison S. L., Patton D. R., 2008, *MNRAS*, 387, 1281
 McGill R., Tukey J. W., Larsen W. A., 1978, *Am. Stat.*, 32, 12
 Navarro J. F., Mosconi M. B., Garcia Lambas D., 1987, *MNRAS*, 228, 501
 Planck Collaboration XIII, 2016, *A&A*, 594, A13
 Planck Collaboration VI, 2020, *A&A*, 641, A6
 Ponman T. J., Bourner P. D. J., Ebeling H., Böhringer H., 1996, *MNRAS*, 283, 690
 Press W. H., Schechter P., 1974, *ApJ*, 187, 425
 Pujol A. et al., 2017, *MNRAS*, 469, 749
 Ragone-Figueroa C., Plionis M., Merchán M., Gottlöber S., Yepes G., 2010, *MNRAS*, 407, 581
 Raouf M., Khosroshahi H. G., Ponman T. J., Dariush A. A., Molaeinezhad A., Tavasoli S., 2014, *MNRAS*, 442, 1578
 Schneider D. P., Gunn J. E., 1982, *ApJ*, 263, 14
 Spergel D. N. et al., 2003, *ApJS*, 148, 175
 Springel V. et al., 2005, *Nature*, 435, 629
 Taverna A., Díaz-Giménez E., Zandivarez A., Joray F., Kanagusuku M. J., 2016, *MNRAS*, 461, 1539
 Tweed D. P., Mamon G. A., Thuan T. X., Cattaneo A., Dekel A., Menci N., Calura F., Silk J., 2018, *MNRAS*, 477, 1427
 Tzanavaris P., Gallagher S. C., Ali S., Miller D. R., Pentering S., Johnson K. E., 2019, *ApJ*, 871, 242
 van den Bosch F. C., 2002, *MNRAS*, 331, 98
 Wiens C. D., Wenger T. V., Tzanavaris P., Johnson K. E., Gallagher S. C., Xiao L., 2019, *ApJ*, 873, 124
 Zandivarez A., Díaz-Giménez E., Mendes de Oliveira C., Ascaso B., Benítez N., Dupke R., Sodré L., Irwin J., 2014a, *A&A*, 561, A71
 Zandivarez A., Díaz-Giménez E., Mendes de Oliveira C., Gubolin H., 2014b, *A&A*, 572, A68

APPENDIX A: COMPACT GROUP VIRIALIZATION REDSHIFT IF THEY REMAIN AS DENSE UNTIL PRESENT

We estimate here the redshift z_{vir} when CGs virialize if they remain at the same physical density until present. The mean density of the CG is

$$\bar{\rho} = \Delta_{\text{CG}} \rho_{\text{crit}}(0) = \Delta(z_{\text{vir}}) \rho_{\text{crit}}(z_{\text{vir}}), \quad (\text{A1})$$

where $\rho_{\text{crit}}(z) = 3H^2(z)/(8\pi G)$ is the critical density. The CG virialization redshift is therefore the solution of

$$\Delta(z) E^2(z) = \Delta_{\text{CG}}, \quad (\text{A2})$$

where $E(z) = H(z)/H_0 = \sqrt{\Omega_m(1+z)^3 + 1 - \Omega_m}$ for a flat Universe with current density parameter Ω_m . According to the values listed in table 5 of Díaz-Giménez et al. (2012), the overdensity of CGs is $\Delta_{\text{CG}} = 3(\mathcal{M}_{\text{VT}}/L_R)L_R/(4\pi r_p^3) = 24\,000$ and $28\,000$, for the median CGs in the 2MASS catalogue (Díaz-Giménez et al. 2012) and mock CGs (from the G11 SAM), respectively (all considered after velocity filtering). Here, we measured the CG density within the sphere of radius equal to the smallest circumscribed radius (this assumes that the typical CG is spherical). Solving equation (A2), we deduce $z_{\text{vir}} = 7.1$ (2MCG) and 7.6 (mock CGs). However, CGs may be more extended along the line of sight than viewed in projection. Adopting a CG radius of $2r_p$ instead of r_p , the overdensities are eight times lower, and the virialization redshifts are now $z_{\text{vir}} = 3.0$ and 3.2 , respectively.

APPENDIX B: ANALYSIS OF CGS IN ALL SEMI-ANALYTICAL MODELS

B1 Assembly histories of CA CGs

For a more detailed analysis, we defined CA subclasses as follows:

- (i) **3+1**: $r_{\text{max}} < D_*$ and $r_{\text{min}} < d_*$ and $r_{\text{max}3} \leq d_*$,
- (ii) **2+2**: $r_{\text{max}} < D_*$ and $r_{\text{min}} < d_*$ and $r_{\text{max}3} > d_*$ and $r_{ij} \leq d_*$,
- (iii) **2+1+1**: $r_{\text{max}} < D_*$ and $r_{\text{min}} < d_*$ and $r_{\text{max}3} > d_*$ and $r_{ij} > d_*$,
- (iv) **Fake**: $r_{\text{max}} \geq D_*$ or $r_{\text{min}} \geq d_*$,

where r_{max} and r_{min} are the maximum and minimum inter-particle separation using the four members of the group, respectively, $r_{\text{max}3}$ is the maximum inter-particle separation between the three closest members of the group, r_{ij} is the inter-particle separation between the two members that do not define the pair with r_{min} , and the thresholds

Table B1. Number of $z = 0$ CAs and percentages within each CA subclass.

SAM	CAs				
	#	% Fake	% 3+1	% 2+2	% 2+1+1
All	4423	27 ± 1	52 ± 1	8 ± 1	13 ± 1
DLB	1320	28 ± 2	52 ± 3	7 ± 1	13 ± 2
G11	1040	24 ± 3	54 ± 3	7 ± 2	15 ± 2
G13	710	28 ± 3	48 ± 4	9 ± 2	15 ± 3
H15	579	30 ± 4	47 ± 4	8 ± 2	15 ± 3
GII	774	25 ± 3	56 ± 3	9 ± 2	10 ± 2

Note. Each percentage p is quoted as $p \pm ci$ where ci is the 95% binomial confidence interval computed as $\pm(1.96 \times \sqrt{f(1-f)/N_{\text{CG}}}) \times 100$ where $f = p/100$.

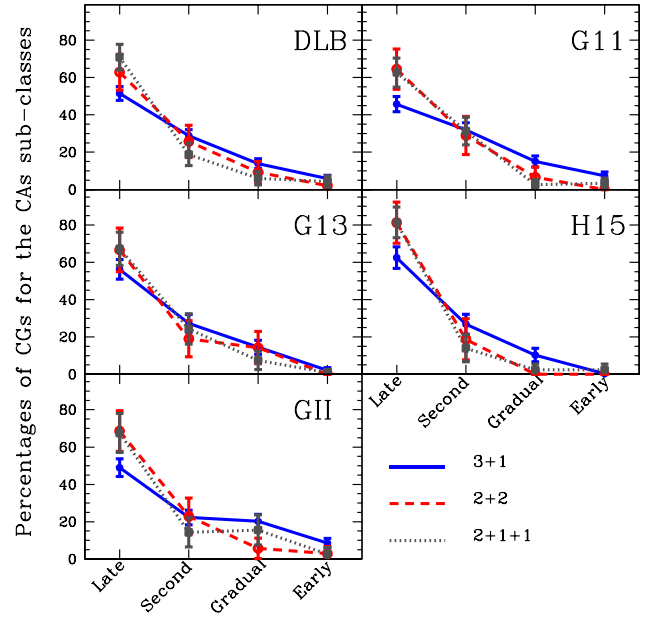


Figure B1. Same as Fig. 6, but only for the four-galaxy CGs that are chance alignments, split by subclass.

are $D_* = 1 h^{-1}$ Mpc and $d_* = 200 h^{-1}$ kpc. Table B1 displays the percentages of the different CA subclasses for each SAM.

We checked how the assembly histories differ among the different subclasses of CAs (excluding Fakes). Fig. B1 shows the percentages of CG4s for the CA subclasses as a function of assembly class. All the CA subclasses roughly follow the general trend previously observed for the full sample of CAs, with the main contribution to Gradual and Early classes of the CAs coming from the dominant ‘3+1’ subclass. The subclasses with one or two galaxy pairs are mainly recently formed in all SAMs. In summary, the richer the subsystem, the earlier it tends to assemble, from pairs (2+2 or 2+1+1 CAs) to triplets (3+1 CAs) to quartets (Reals).

Interestingly, the key galaxy of a CA, which by definition is the galaxy with the fewest orbits, is not necessarily an outlier at $z = 0$ (for 3+1 CAs) or one of them (for 2+2 or 2+1+1 CAs). So the classification of CA assembly histories, which is a function of the orbit of the key galaxy, is not necessarily tied to an outlier but to one of the galaxies of the physical subsystem (i.e. triplet in a 3+1 CA). However, the key galaxy of a CA is more likely to be an outlier galaxy, since to first order, galaxies further out live in lower mean densities, hence have the longest orbital times and the fewest number of orbits. Nevertheless, the fraction of CAs classified as Late or Second is less than two-thirds. On the other hand, finding that the 3+1 CAs are the main contributor to Early is expected, because 3+1 CAs have only one outlier and are thus less likely to have their key galaxy be an outlier than 2+2 or 2+1+1 CAs.

B2 Observational properties versus SAM

Fig. B2 shows the properties of CGs in each assembly class for the SAMs of DLB, G11, G13, and H15.

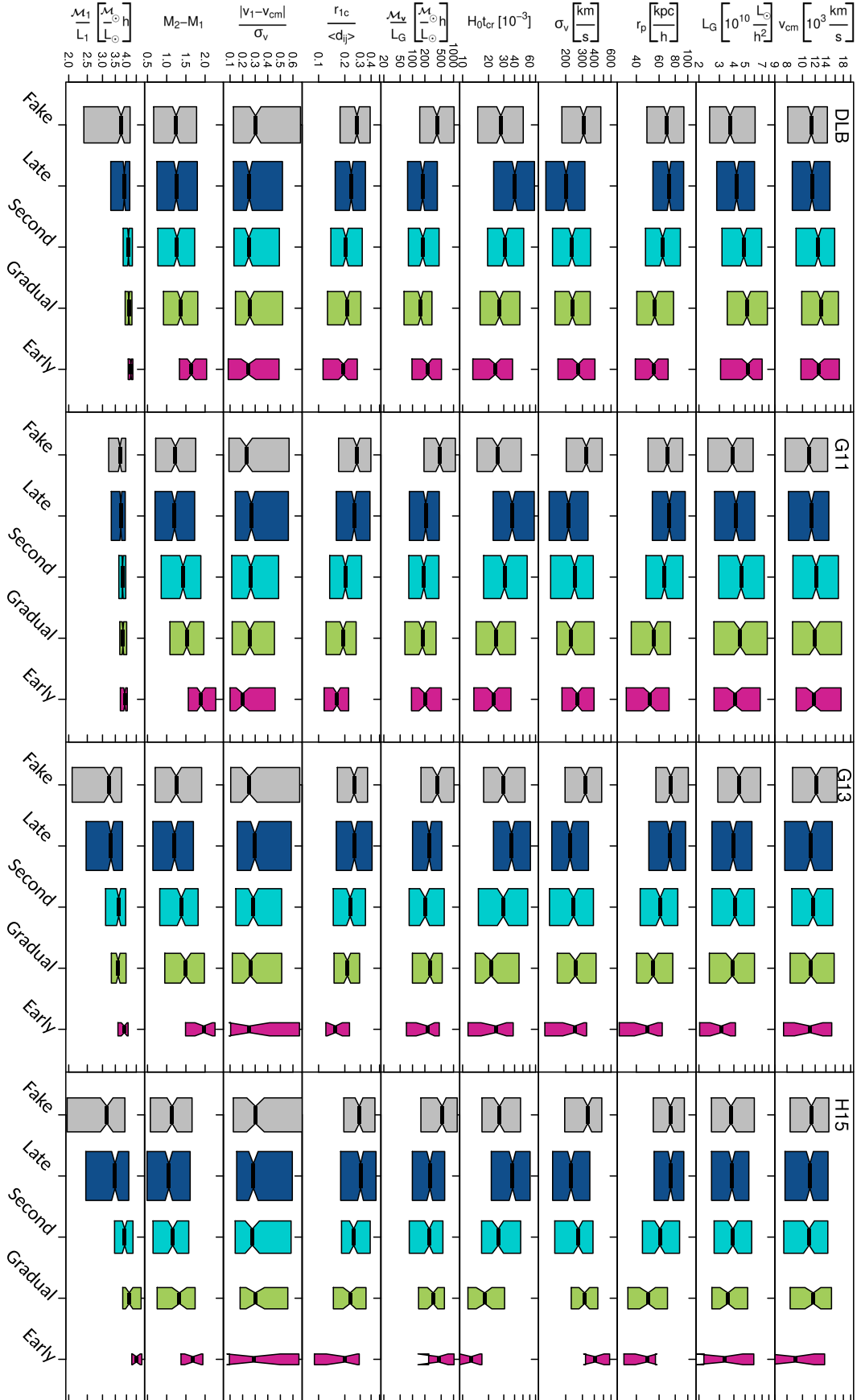


Figure B2. Same as Fig. 9, but for the CGs built from the four other semi-analytical models.